Hydrometallurgy 191 (2020) 105184

Contents lists available at ScienceDirect

Hydrometallurgy

journal homepage: www.elsevier.com/locate/hydromet

The leachability of a ternary $CaO-Al_2O_3-SiO_2$ slag produced from smelting-reduction of low-grade bauxite for alumina recovery

Fabian Imanasa Azof[a,*], Michail Vafeias[b], Dimitrios Panias[b], Jafar Safarian[a]

[a] Norwegian University of Science and Technology (NTNU), Department of Materials Science and Engineering, Trondheim, Norway
[b] National Technical University of Athens (NTUA), School of Mining and Metallurgical Engineering, Athens, Greece

ARTICLE INFO

Keywords:
Low-grade bauxite
Smelting-reduction
Aluminate slag
Alumina
Leachability
Leaching residue

ABSTRACT

A combination of smelting-reduction of bauxite and leaching treatment of the produced slag for alumina recovery is known as the Pedersen process. The process is considered to be more sustainable for producing metallurgical-grade alumina than the Bayer process as it does not produce bauxite residue (red mud), which is one of the most abundant industrial byproducts in the world. In this work, the leachability of a ternary $CaO-Al_2O_3-SiO_2$ slag produced from smelting-reduction of low-grade bauxite has been studied. The obtained calcium aluminate-slag consists of $Ca_{12}Al_{14}O_{33}$ and $CaAl_2O_4$ phases with minor amounts of complex oxide phases. A leaching series have been carried out at different temperatures, $Na_2O_{(carbonate)}$:$Na_2O_{(caustic)}$ concentration ratios. The composition of solids and leaching liquors were analyzed for measuring the recovery of the aluminum and silicon. The results show that the highest aluminum extraction extent in the current study is 46.7%, which is achieved at a temperature of 75 °C, 1 atm, in 60 g/L $Na_2O_{(carbonate)}$ solution, in 30 min of leaching time. A passive calcium-containing layer at the slag's surface acts as a mass transfer barrier for the reactants and products of the leaching reactions, making their diffusion the rate-limiting step. A high concentration of $Na_2O_{(caustic)}$ may decrease the aluminum extraction of the slag as a result of insufficient carbonate anions in the system, where the dissolved aluminum reacts with the calcium cations and produce $3CaO{\cdot}Al_2O_3{\cdot}6H_2O$ phase.

1. Introduction

Excessive production of bauxite residue (red mud), which is estimated 150 million tonnes annually in 2017 (Tsesmelis, 2017) becomes one of the major concerns amongst alumina producers. The severe accidents on red mud dams occurred during the last decades (Norway's Norsk Hydro apologises for spills in Brazil river_2018.pdf WWW Document, 2018; Outrage as plant bosses acquitted over fatal toxic spill in Hungary WWW Document, 2016) boosted many research projects on red mud valorization worldwide. However, according to recent literature (Azof et al., 2018), none of them have been scaled up to commercial production due to economic reasons and particular challenges. In 1927, a Norwegian metallurgist named Harald Pedersen (1927) had patented a process for manufacturing aluminum hydroxide from ferruginous bauxite that was based on the combination of both pyro- and hydrometallurgical processes. The schematic flow sheet of the original Pedersen process is shown in Fig. 1. The process produces pig iron, metallurgical-grade alumina, and an inert leaching residue called grey mud, which can be used in the agriculture industry as a fertilizer or soil improver, and one of rare earth elements potential resource (Vafeias et al., 2018). Thus, the Pedersen process eliminates the red mud problem as encountered in the Bayer process.

The amount of the red mud produced in the Bayer process is positively related to the mass concentration of iron-bearing phases in the bauxite, which is evident as the composition of the red mud is dominated by iron oxide phases (Safarian and Kolbeinsen, 2016a). In alumina industries, bauxite with relatively low Al_2O_3/SiO_2 mass ratio is considered as low-grade bauxite. Meanwhile, bauxite with low Al_2O_3/Fe_2O_3 mass ratios can be regarded as low-grade bauxite as well (Blake et al., 1966). Although from a technical point of view bauxites with low Al_2O_3/Fe_2O_3 mass ratios can be treated with the Bayer process, however, from an economic point of view their treatment is unfavorably facing additionally the challenge of disposal of vast amounts of red mud produced as mentioned earlier. On the contrary, the Pedersen process seemed to be more advantageous for the treatment of low-grade bauxites. A relationship between the content of alumina and iron oxides in a typical bauxite and laterite deposit is reconstructed from Nielsen (1978) in Fig. 2, which shows that the Pedersen process is suitable for all grades of deposit in the particular compositions.

Furthermore, Smith (2009) states that bauxite with an Al_2O_3/SiO_2

* Corresponding author.
E-mail address: fabian.i.azof@ntnu.no (F.I. Azof).

https://doi.org/10.1016/j.hydromet.2019.105184
Received 20 April 2019; Received in revised form 20 September 2019; Accepted 17 October 2019
Available online 28 October 2019

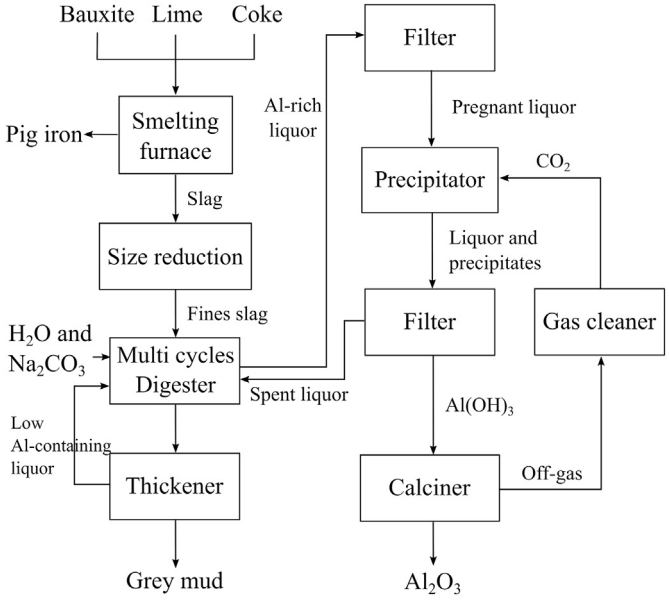

Fig. 1. A schematic flow sheet of the original Pedersen process.

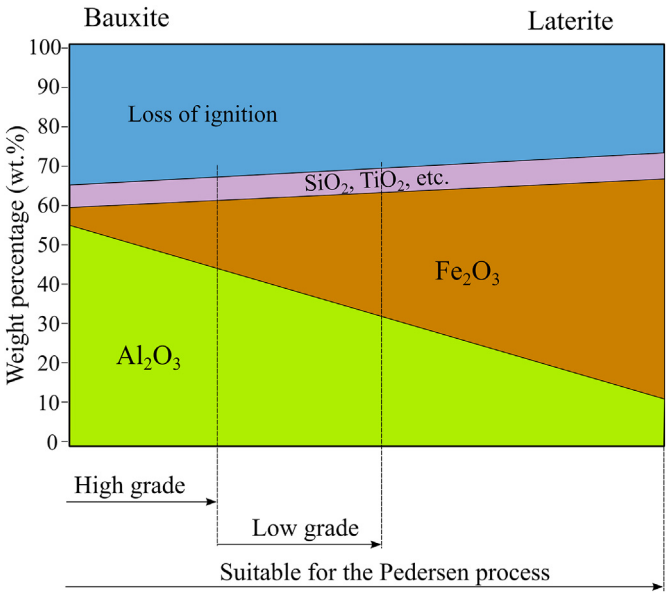

Fig. 2. The relationship between the content of alumina and iron oxide in a bauxite and laterite deposit, as was reconstructed after Nielsen (1978).

mass ratio < 6.25 or with a reactive silica content higher than 8 wt% is regarded as low-grade one, and is considered uneconomic for the Bayer process. This typical bauxite is not favorable for both the Bayer and the Pedersen process due to the silicon-bearing phases that may dilute into the solution during the digestion that needs a further desilication treatment. Table 1 shows the chemical composition of bauxites that were taken from several locations in the world.

Moreover, Fig. 3 shows the distribution of bauxites based on Al_2O_3/SiO_2 and Al_2O_3/Fe_2O_3 mass ratios that correspond to the bauxite ores in Table 1. In Fig. 3, we only consider the ratio between three major compounds, which are Al_2O_3, SiO_2, Fe_2O_3, and do not include TiO_2 as it has a relatively low concentration; < 4 wt%.

Norwegian University of Science and Technology (NTNU) through research domain 5-Materials and Society in SFI-metal production and National Technical University of Athens (NTUA) have initiated and started preliminary work on reviving the Pedersen process. The European Union under Horizon 2020 program also has launched ENSUREAL project (www.ensureal.com) that was based on the same process, where the two universities were also involved. Most of the authors' previous studies (Azof et al., 2018; Safarian, 2018a, 2018b; Safarian and Kolbeinsen, 2016a, 2016b; Sellaeg et al., 2017) focused on the pyro-metallurgical part, especially in the smelting-reduction process of low-grade bauxite ores. Our several studies (Azof et al., 2017, 2019a, 2019b) in the hydro-metallurgical part of the Pedersen process were mainly focused on the leaching characteristics of synthetic $CaO-Al_2O_3$ slags. In the meantime, there has been limited information provided from the literature regarding the leaching characteristics of ternary $CaO-Al_2O_3-SiO_2$ slag produced from the smelting-reduction of bauxite, as well as the physicochemical characteristics of residue (grey mud) generated from the leaching process. Therefore, in the current work, we study the leachability of a calcium aluminum silicate slag in different leaching conditions (e.g., temperature, Na_2CO_3-NaOH concentration of the leaching solution) for alumina recovery and investigate the chemical properties and morphology of grey mud.

2. Theoretical calculation

In the literature (Azof et al., 2018), the smelting-reduction process, which uses a mixture of lime, coke, and bauxite ore with CaO/Al_2O_3 molar ratios of 1.0–1.7 as the feed material, produces a calcium aluminate slag that contains leachable phases in a sodium carbonate solution. The known leachable phases are $CaAl_2O_4$ (denoted as CA) and $Ca_{12}Al_{14}O_{33}$ (denoted as $C_{12}A_7$) (Azof et al., 2017; Blake et al., 1966; Lundquist and Leitch, 1963a, 1963b). However, other calcium-aluminum-silicate phases, i.e., $CaAl_2SiO_6$ (denoted as CAS), $Ca_2Al_2SiO_7$ (denoted as C_2AS), may also coexist in the slag depending on the nature of silicon content of the bauxite ore.

The leaching reactions of CA and $C_{12}A_7$ phase in Na_2CO_3 solution and their Gibbs energy change values at room temperature can be written as follows (Azof et al., 2017; Blake et al., 1966; Lundquist and Leitch, 1963a, 1963b):

$$CaAl_2O_{4(s)} + Na_2CO_{3(aq)} = 2NaAlO_{2(aq)} + CaCO_{3(s)}$$
$$\Delta G°_{25°C} = -53.6\ kJ/molCaAl_2O_4 \quad (1)$$

$$Ca_{12}Al_{14}O_{33(s)} + 12Na_2CO_{3(aq)} + 5H_2O_{(l)} = 14NaAlO_{2(aq)} + 12CaCO_{3(s)} + 10NaOH_{(aq)}$$
$$\Delta G°_{25°C} = -745.2\ kJ/molCa_{12}Al_{14}O_{33} \quad (2)$$

Both Reactions (1) and (2) show that the formation of $NaAlO_2$ aqueous phase is favorable at room temperature. By using HSC™ v.9 equilibrium compositions module, we calculate the thermo-chemical equilibrium of CA and $C_{12}A_7$ leaching reactions at different temperatures. The result is shown in Fig. 4. The amount of input and list of output species used in the calculation are enclosed as a supplementary material of the article. The selection is based on the possible phases that may form in an aqueous solution that consists of Al–O–H–Ca–C–Na element according to the software's database.

As seen in Fig. 4, CA and $C_{12}A_7$ have a negligible amount in the equilibrium condition at the respected range of temperatures, which indicates that the phases are leachable in solution. The solid product of the leaching reactions in equilibrium, $CaCO_3$, has a constant amount regardless of the temperature.

3. Experimental

In this section, we describe the materials preparation, characterization of the samples, and leaching equipment and process parameters.

3.1. Slag preparation

The main material used in the current study is a slag that was produced by a smelting-reduction process of a mixture of bauxite, coke,

Table 1
Chemical composition of bauxites at several locations in the world.

No	Country, location	Reference	Composition (wt%)				
			Al_2O_3	SiO_2	Fe_2O_3	TiO_2	LOI
1	Greece, Parnassos-Ghiona	(Laskou et al., 2005)	62.5	2.1	19.5	2.9	13.0
2	Former Soviet Union, Severouraisk	(Hudson et al., 2000)	58.0	6.7	15.9	2.6	16.9
3	France, Southern Districts	(Hudson et al., 2000)	55.8	4.5	22.1	2.8	14.8
4	Former Yugoslavia, Mostar	(Hudson et al., 2000)	54.2	4.1	22.1	2.8	16.9
5	Indonesia, Bintan	(Hudson et al., 2000)	53.3	3.9	12.1	1.6	29.1
6	Iran, Sar-Faryab	(Zarasvandi et al., 2010)	52.5	6.4	19.7	3.3	18.1
7	Brazil, Trombetas	(Hudson et al., 2000)	51.8	5.1	13.9	1.2	28.0
8	Hungary, Halimba	(Hudson et al., 2000)	50.4	6.4	22.8	2.8	17.6
9	Guinea, Friguia	(Hudson et al., 2000)	49.5	6.2	14.3	1.6	28.4
10	Jamaica, Clarendon	(Hudson et al., 2000)	49.0	2.7	18.0	2.4	28.0
11	India, Orissa	(Hudson et al., 2000)	47.7	2.8	23.2	1.1	25.1
12	China, Guangxi	(Liu et al., 2009)	54.8	6.4	18.9	NA	NA
13	Guyana, Mackenzie	(Hudson et al., 2000)	59.2	4.9	2.9	2.4	30.5
14	Surinam, Onverdacht	(Hudson et al., 2000)	59.1	4.3	3.1	2.5	31.0
15	Australia, Weipa	(Hudson et al., 2000)	58.8	4.6	7.0	2.5	27.2
16	Guinea, Boke	(Hudson et al., 2000)	56.5	1.5	8.0	3.7	30.3
17	Surinam, Moengo	(Hudson et al., 2000)	53.8	4.2	10.4	2.8	28.8
18	China, Guizhou	(Liu et al., 2009)	65.7	9.0	5.5	NA	NA
19	China, Shanxi	(Liu et al., 2009)	62.3	11.6	5.8	NA	NA
20	China, Henan	(Liu et al., 2009)	65.3	11.8	3.4	NA	NA
21	China, Shandong	(Liu et al., 2009)	55.5	15.8	8.8	NA	NA
22	United States, Arkansas	(Hudson et al., 2000)	51.3	11.3	6.6	2.2	28.6
23	Australia, Darling Range	(Hudson et al., 2000)	36.9	26.4	16.4	1.1	19.2
24	Iran, Kanisheeteh	(Calagari and Abedini, 2007)	33.9	25.8	27.3	3.9	9.2
25	Indonesia low-grade, Bintan	(Kusrini et al., 2018)	35.5	33.7	29.7	1.1	NA

and lime from our previous study (Azof et al., 2018). The mixture was melted in an induction furnace at 1650 °C for one hour, then slowly cooled down to the room temperature. The iron oxide and other oxides in the bauxite were reduced to some extent and yield pig iron. On the other hand, the solidified oxides that mainly comprises of CaO–Al_2O_3–SiO_2 compound is the slag. The composition of bauxite and slag are presented in Table 2. The slag was pulverized by a RETSCH™ ring mill for 30 s in 700 rpm, which gives D_{50} 73.6 μm for the particle size, as measured by a laser particle analyzer after 2 min of ultrasound vibration.

3.2. Characterization of materials

3.2.1. Characterization of solids

We used non-destructive X-ray Fluorescence (XRF) SPECTRO XEPOS™ to measure the chemical composition of the grey mud produced from the leaching treatment. The Backscattered Electron (BSE) images and the multi-point Energy Dispersive Spectroscopy (EDS) of both the slag and grey mud were performed by using Hitachi SU6600™ Scanning Electron Microscope (SEM). Moreover, an X-ray elemental mapping of the grey mud's cross section was carried out using JEOL JXA- 8500F Electron Probe Micro Analyzer (EPMA) with Wavelength Dispersive X-ray Spectrometer (WDS). For mineralogy phase

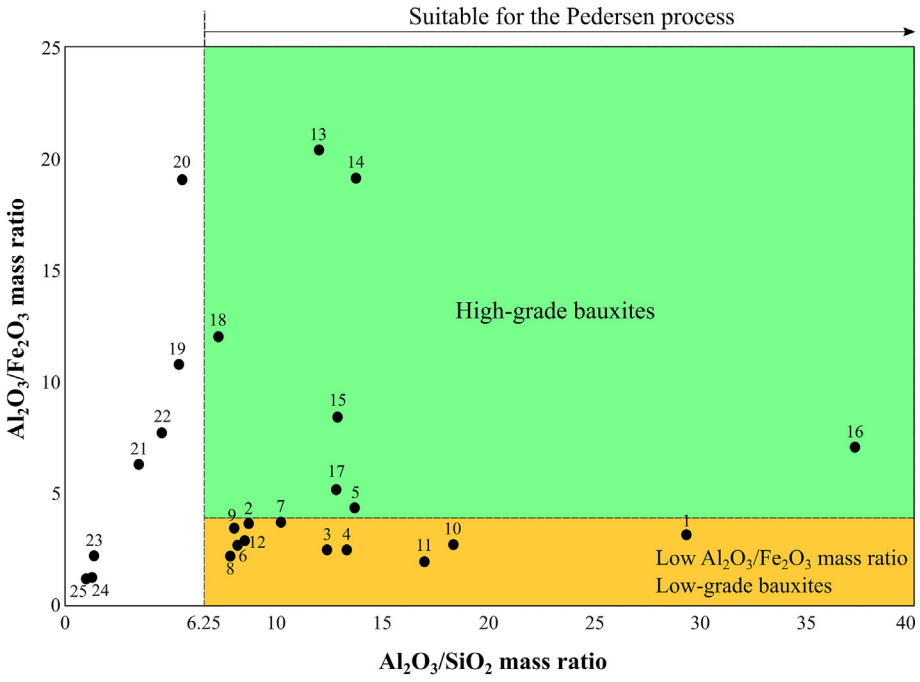

Fig. 3. Distribution of bauxite ores that is based on Al_2O_3/SiO_2 and Al_2O_3/Fe_2O_3 mass ratios. The ores in the green, gold, and white-colored areas indicate that they have relatively high Al_2O_3/SiO_2 and Al_2O_3/Fe_2O_3, low Al_2O_3/Fe_2O_3, and low Al_2O_3/SiO_2 mass ratios, respectively. (For interpretation of the references to colour in this figure legend, the reader is referred to the web version of this article.)

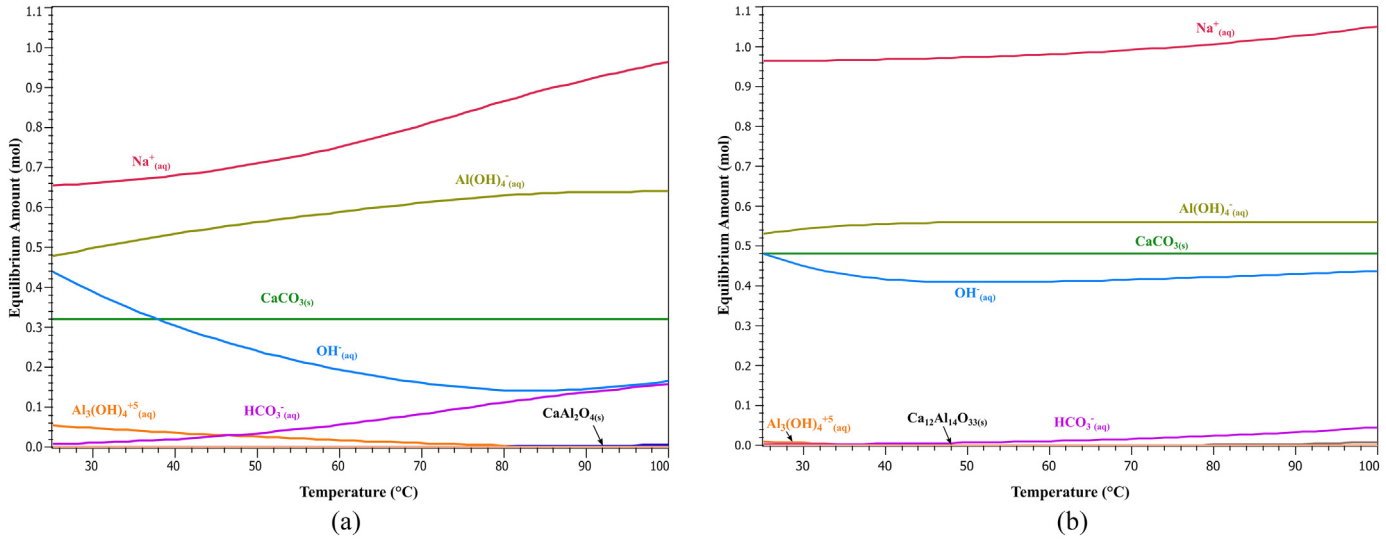

Fig. 4. The thermochemical simulation of the equilibrium amount of species in an aqueous solution at a temperature at 25–100 °C and 1 atm that corresponds to: (a) the leaching reaction of CA, (b) the leaching reaction of $C_{12}A_7$ phases.

Table 2
The composition of low-grade bauxite and slag.

Materials	Constituents (wt%)					
	Al_2O_3	CaO	SiO_2	TiO_2	Fe_2O_3	MgO
Bauxite	65.4	4.4	4.1	3.2	22.7	0.2
Slag	46.1	48.1	2.3	1.8	0.9	0.5

identification, we used Bruker D8 A25 DaVinci™ X-ray Diffractometer (XRD) with CuKα radiation, 10 to 75 deg. diffraction angle, 0.01 deg. step size, and 2.5 deg. for both primary and secondary soller slits.

3.2.2. Analysis of liquor samples

The liquor samples of the pregnant liquid solution (PLS) were taken after separating the solid and liquid by using an ashless grade of quantitative filter paper. Inductively Coupled Plasma Optical Emission Spectrometry (ICP-OES) was used to measure the concentration of aluminum and silicon of the PLS for observing the recovery of aluminum and silicon from the slag after the leaching treatment.

3.3. Leaching setup and process parameters

The leaching treatment was performed inside a Parr 4563 mini reactor, which is an Inconel alloys-based vessel with 600 mL capacity that is resistant to chemical attack. The reactor was heated through a conduction heating. It has a lid that is made of Teflon, which is fitted with a condenser for condensing the water vapors that allows the pressure inside of the reactor remained in ambient pressure, and at the same time keeps the liquid-solid (L/S) weight ratio of the system relatively constant. The temperature was measured with a Pt thermocouple and the stirring was performed through a mechanical stirrer. The thermocouple, stirrer, and heater were connected to Parr 4841, a Programmable Logic Controller (PLC), to set and measure the necessitate parameters during the leaching treatment. A schematic of the leaching setup is shown in Fig. 5.

The leaching solution used in this study has a constant concentration of 60 g/L Na_2O, which was made by mixing distilled water, Na_2CO_3 powder and NaOH pellet with 99.8 wt% and 99.0 wt% purity, respectively. The dissolved Na_2CO_3 and NaOH give an extent of Na_2O concentration of the solution that can be denoted as $Na_2O_{(carbonate)}$ and $Na_2O_{(caustic)}$, respectively. Moreover, the concentration mass ratio of $Na_2O_{(carbonate)}$ to $Na_2O_{(caustic)}$ in the solution was varied from 100:0, 85:15, 75:25, and 50:50. By this definition, a leaching solution with 0 wt%$Na_2O_{(caustic)}$ means that the solution contains 60 g/L of $Na_2O_{(carbonate)}$ (denoted as 100 wt% $Na_2O_{(carbonate)}$) and has no $Na_2O_{(caustic)}$. Also, using the same definition, a leaching solution with 50 wt%$Na_2O_{(caustic)}$ means that the solution consists of 30 g/L of $Na_2O_{(caustic)}$ and $Na_2O_{(carbonate)}$ each. The L/S mass ratio was kept at 20:1, and the leaching temperature variations, pressure, and leaching time were 45, 60, 75 °C, 1 atm, and 30 min, respectively.

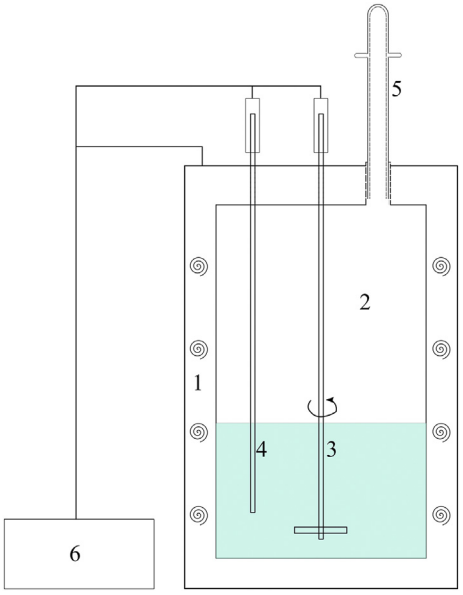

Fig. 5. A schematic of the leaching setup. Legend: 1. Heating element; 2. Inconel-based reactor; 3. Impeller; 4. Thermocouple; 5. Condenser; 6. Programmable Logic Controller (PLC).

4. Results and discussion

This section shows the results and discussion about the characterization of the slag before and after the leaching treatment, slag's leachability in different temperatures and concentration ratios of $Na_2O_{(carbonate)}$: $Na_2O_{(caustic)}$, and characteristics of the grey mud.

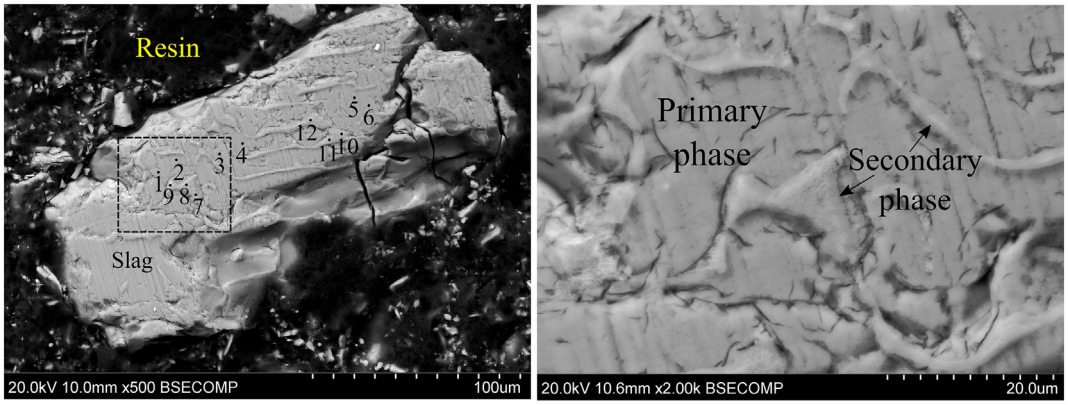

Fig. 6. BSE cross-sectional images of the slag in (a) 500× magnification and (b) 2000× magnification.

4.1. Characteristics of the slag

As seen previously in Table 2, the slag primarily consists of CaO, Al_2O_3, and relatively low concentration of SiO_2, TiO_2, and Fe_2O_3. Based on our previous X-ray Diffraction (XRD) analysis of the slag (Azof et al., 2018), the slag is dominated by $C_{12}A_7$ phase, while minor phases are CA and $Ca_5Al_6O_{14}$ (denoted as $5CaO{\cdot}3Al_2O_3$ or C_5A_3). Fig. 6(a) and (b) show the BSE cross-sectional image of the slag in 500× and 2000× magnification, respectively.

In Fig. 6(b), there are only two distinct phases that can be identified clearly, which can be denoted as a primary and secondary phase. The primary and secondary notations used in this study referring to their relative amount of each phase, which means that the primary phase is considered as a phase that has a higher amount compared to the secondary one. Moreover, Table 3 gives the EDS point analysis that corresponds to the numbers in Fig. 6(a). As seen, the primary phase consists of calcium and aluminum with 39.7 and 31.8 wt% on average, respectively, with no available result on Si and Ti element. However, later in a result of the WDS and X-ray mapping elements of the cross-section of grey mud using EPMA, we can see that Si and Ti also present in a low concentration on the primary phase. This small variance of elemental composition results may happen due to the different characterization techniques applied.

Furthermore, the secondary phase consists of 39.1 wt% Ca, 23.8 wt % Al, 3.7 wt% Si, and 3.4 wt% Ti, on average. The average of Ca/Al mass ratio of primary and secondary phase is 1.2 and 1.6, respectively. Based on the similarity of Ca/Al mass ratio between primary and $C_{12}A_7$ (Ca/Al mass = 1.3), we may conclude that the primary phase is the $C_{12}A_7$ phase. While the secondary phase is a calcium-alumina-silica-titanate bearing phase that was not detected on our previous XRD results, which is likely due to its low amount.

Table 3
The composition of the slag under different EDS points.

Phase	Location	Elements (wt%)					
		Ca	Al	Si	Ti	O	Ca/Al mass ratio
Primary	Point 1	43.1	28.1	NA	NA	28.8	1.5
	Point 2	38.1	31.5	NA	NA	30.4	1.2
	Point 3	39.4	32.9	NA	NA	27.7	1.2
	Point 4	39.0	32.1	NA	NA	28.9	1.2
	Point 5	39.8	33.3	NA	NA	26.9	1.2
	Point 6	38.6	32.9	NA	NA	28.5	1.2
	Average	39.7	31.8	NA	NA	28.5	1.2
Secondary	Point 7	36.6	25.1	3.7	3.4	31.2	1.5
	Point 8	39.6	22.6	4.1	3.6	30.1	1.8
	Point 9	37.9	24.2	3.8	3.6	30.5	1.6
	Point 10	41.4	21.8	4.2	3.6	29.0	1.9
	Point 11	39.4	23.4	3.7	3.6	29.9	1.7
	Point 12	39.9	25.8	2.7	2.3	29.3	1.5
	Average	39.1	23.8	3.7	3.4	30.0	1.6

4.2. Leachability of the slag

The subsection of leachability of the slag covers the aluminum and silicon recoveries based on the leaching series that was carried out. Also, it includes a thermodynamic perspective of the effect of different $Na_2O_{(carbonate)}$: $Na_2O_{(caustic)}$ concentration ratios to the aluminum recovery.

4.2.1. Aluminum and silicon extraction

A ternary $CaO\text{-}Al_2O_3\text{-}SiO_2$ phase diagram is shown in Fig. 7. It is shown the area of preferred slag compositions that are easily soluble in sodium carbonate solutions (green area) according to Blake et al. (1966). The calcium aluminate phases that are present in this area are only the CA as well as $C_{12}A_7$. Moreover, two red dotted lines have been drawn inside the green area representing the optimum slag compositions according to the Company, Norsk Aluminium (1944a,b). The line located closer to the $CaO\text{-}SiO_2$ axis represents a calcium aluminate slag with high silica content (> 10%) while the other represents a calcium aluminate slag with low silica content (< 10%). Finally, a yellow point shows the position of the studied slag in the ternary phase diagram after its normalization. For the normalization the lime reacted with TiO_2 was subtracted from the total CaO content of the slag assuming the formation of $CaO{\cdot}TiO_2$ phase.

As is seen, the composition of studied slag is located in the green area with the leachable slags and very close to the area of $C_{12}A_7$ phase, even though it is not located on one of the red lines showing the optimum compositions according to the Norsk Aluminium patent. An investigation about the optimum leach composition as claimed by the patent was reported elsewhere (Fursman et al., 1968).

Regarding the leachability of the slag, concentrations of Al and Si in the PLS after series of leaching are shown in Fig. 8. The results show that leaching solutions with 100 wt%$Na_2O_{(carbonate)}$ produce 5.4–5.7 g/L of aluminum in the PLS. Whereas, lower concentrations of aluminum between 2.3 and 4.1 g/L are produced from solutions with 50 wt% $Na_2O_{(caustic)}$ at any studied temperatures. Furthermore, silicon concentration in the PLS is ranging from 0.1–0.2 g/L. As shown in the figure, the higher aluminum concentration of the solution is, the higher concentration of silicon will be. It is also worth to note, the aluminum and silicon concentrations from solutions that were treated at 60 and 75 °C show similar results. We may suggest that for energy consumption and aluminum yield considerations in the current study, leaching at 60 °C is preferable than leaching at 75 °C.

In addition, the aluminum and silicon extraction of the slag after a

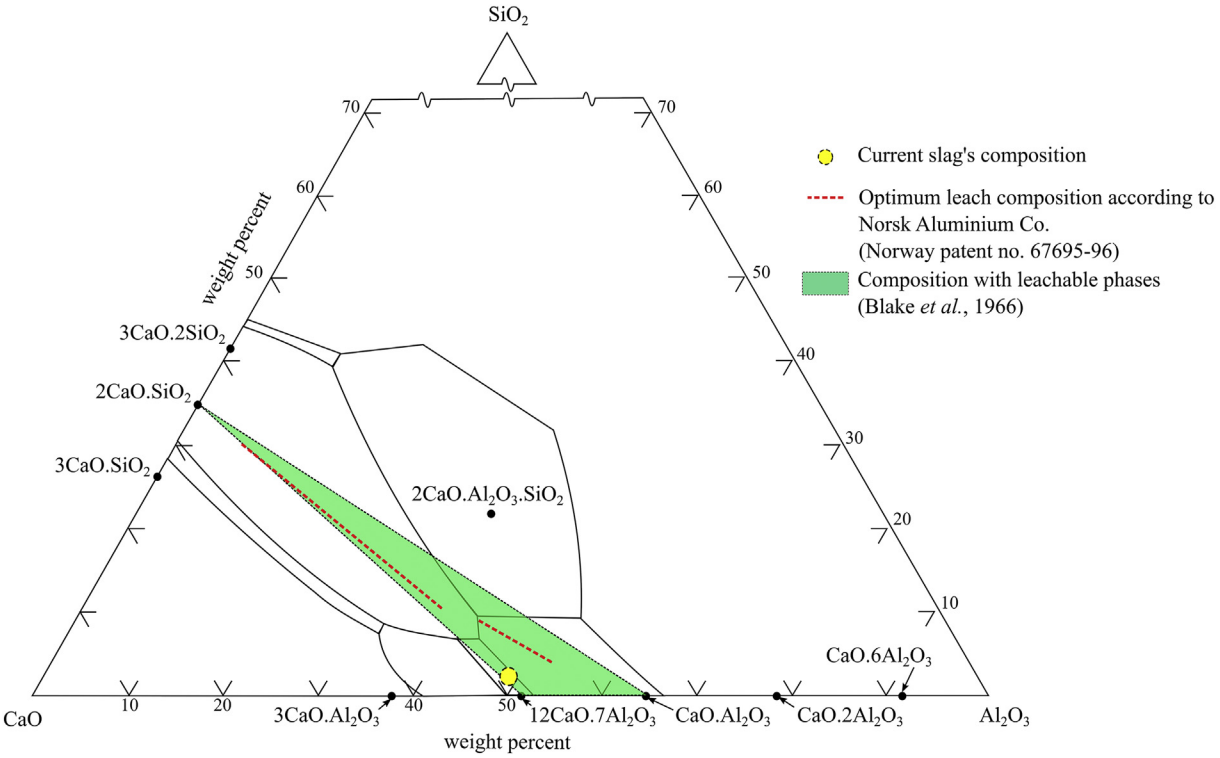

Fig. 7. A ternary CaO-Al_2O_3-SiO_2 phase diagram. A yellow dotted-circle indicating the composition of current slag, a red dash-line showing an optimum leach composition according to Norsk Aluminum Co. at low and high-silica content, and a light green area showing a composition that may form leachable phases. (For interpretation of the references to colour in this figure legend, the reader is referred to the web version of this article.)

series of leaching experiments is shown in Fig. 9(a) and (b), respectively. The highest aluminum extraction extent in the current study is 46.7%, which is achieved at a temperature of 75 °C and 1 atm in 100% $Na_2O_{(carbonate)}$ solution. While the lowest one is 18.9% that is attained at 45 °C in 50:50 of $Na_2O_{(carbonate)}$:$Na_2O_{(caustic)}$ concentration.

In Fig. 9(a), it is evident that the increasing of $Na_2O_{(caustic)}$ concentration ratio leads to the decreasing of aluminum extraction extent. The phenomena are apparent, as the increasing ratio of $Na_2O_{(caustic)}$ means that the available $Na_2O_{(carbonate)}$ in the solution is decreasing. The availability of $Na_2O_{(carbonate)}$ is necessary to proceed with the leaching reactions. Also, we find that the leaching at a high $Na_2O_{(caustic)}$ concentration generates grey mud that contains aluminum hydrated phase that results in loss of aluminum in the PLS, which will be discussed further in Section 4.3.2, which is on the phase of grey mud. Moreover, it seems that the differences in temperature give a mild effect on the extent of aluminum extraction. As the leaching time is

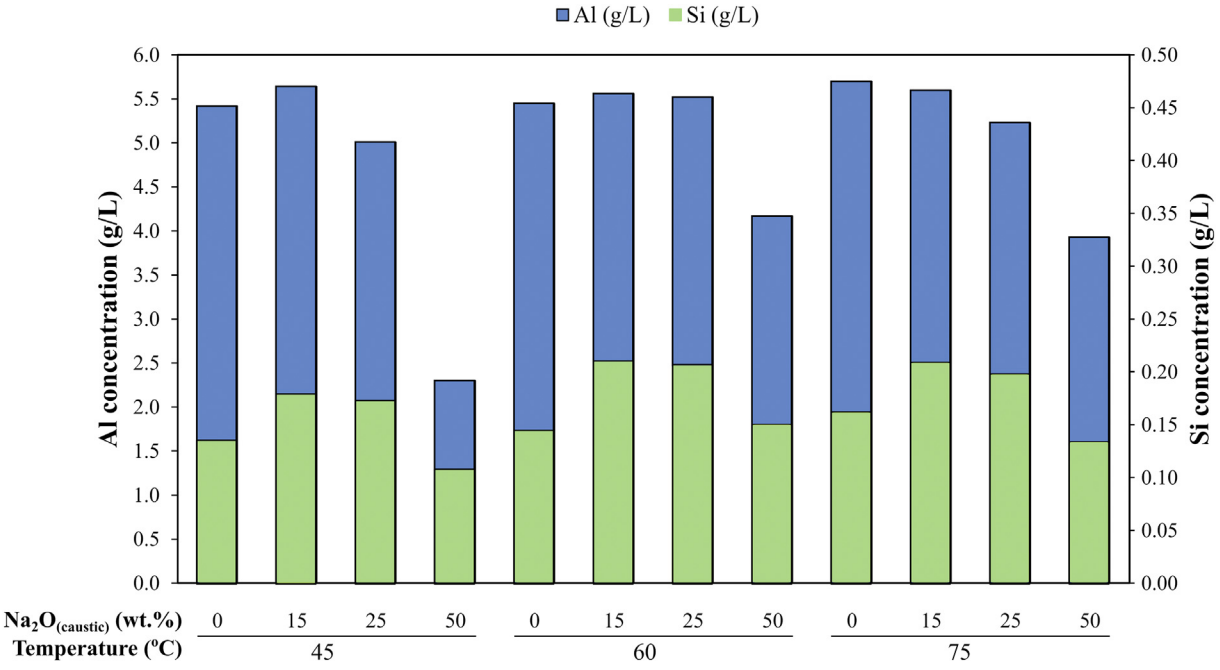

Fig. 8. Aluminum and silicon concentrations in the PLS obtained from different leaching conditions.

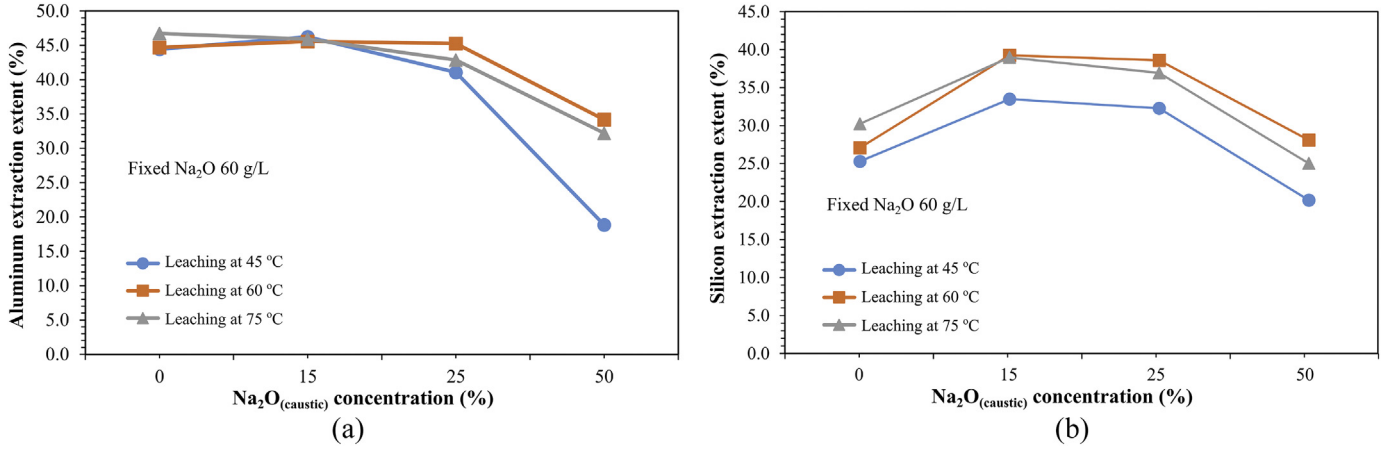

Fig. 9. (a) Aluminum and (b) silicon extraction extent of the leaching of slag. The leaching temperature and pressure are 45, 60, and 75 °C at 1 atm, and the leaching time is 30 min in 60 g/L Na_2O solution with different concentration of $Na_2O_{(caustic)}$.

considerably short (30 min), further experiments with varying more parameters (e.g., leaching time, stirring rate, particle size, L/S, etc.) are necessary to have a better understanding of the leaching kinetics of the slag.

On the other hand, as seen in Fig. 9(b), the silicon dissolution in the PLS substantially increases as the $Na_2O_{(caustic)}$ concentration ratio increases up to 25%, and then it decreases significantly together with the aluminum dissolution as the $Na_2O_{(carbonate)}$:$Na_2O_{(caustic)}$ concentration ratio is 50:50. It is confirmed in the literature (Fursman et al., 1968) that the excessiveness of $Na_2O_{(caustic)}$ concentration increases the silicon dissolution into the PLS, which is in agreement with the result at 15 and 25% of $Na_2O_{(caustic)}$ concentration. However, the mechanism of decreasing the extent of silicon dissolution at 50:50 $Na_2O_{(carbonate)}$:$Na_2O_{(caustic)}$ is unclear. We suggest that it is likely due to the decreasing rate of the main leaching reactions as the silicon in the PLS originates from the depolymerized slag that contains silicon impurity. The leaching mechanism is discussed later in Section 4.3.1.

Furthermore, similar to the aluminum extraction, we find that the leaching temperature gives a modest effect to the silicon dissolution as well. A low leaching temperature is more favorable than a high one to minimize the silicon dissolution in the PLS, which is in agreement with the original Pedersen patent where Pedersen used moderate temperatures for the digestion (Pedersen, 1927).

4.2.2. Effect of the sodium hydroxide concentration

In the original Pedersen (1927) process, it was stated that a "free sodium hydroxide" is needed to prevent the dissolution of silicon during the leaching, and if a larger proportion of "free sodium hydroxide" is used the alumina dissolution decreased. The latter claim is in agreement with the current results, considering the alumina dissolution decreases as the $Na_2O_{(caustic)}$ increases. However, in the current result, we could not observe the effect of "free sodium hydroxide" on the prevention or reduction of the silicon dissolution as the first sentence of the claim stated. Even though as small as 12 g/L of $Na_2O_{(caustic)}$ was added to the solution, the silicon extraction extent increases by approximately 10%, on average.

The discrepancy between the Pedersen patent and the current result might have resulted from the different digestion's concentration, the method applied, and the phase of calcium aluminate used, which can be described as following:

First, in the original Pedersen process, the aqueous solvent is a dilute solution that consists of 18–23 g/L $Na_2O_{(carbonate)}$ in which the amount of "free sodium hydroxide" is about 10 wt% of the amount of total carbonate. Whereas, in the current study, we use up to 60 g/L $Na_2O_{(carbonate)}$, and the addition of NaOH is larger than the Pedersen, which is amounted from 13 to 75 wt% of the total carbonate.

Second, the Pedersen original patent uses two or more countercurrent leaching steps, where an excess of slag is charged to the first leachate to lower the SiO_2 content in the final solution. Also, the filtrate from the CO_2 precipitation stage that contains a high concentration of Na_2CO_3 is charged to the second or final extraction stage, which allows the ratio of free Na_2CO_3 over the calcium aluminate is maintained. On the other hand, in the current study, we performed a single leaching stage experiment in a relatively shorter leaching time compared to the original patent.

Third, according to Fursman et al. (1968), the $Na_2O_{(caustic)}$ concentration of the leachate shall be controlled as if it excessive then the silicon dissolution increases, and when it is too low, the $Al_2O_3{\cdot}H_2O$ precipitates and become lost in the grey mud. They claimed that introducing CO_2 gas during the leaching would be necessitated to control the $Na_2O_{(caustic)}$ or $OH^-_{(aq)}$ level, as shown in the Reaction (3).

$$CO_{2(g)} + 2OH^-_{(aq)} = CO_3^{2-}{}_{(aq)} + H_2O_{(l)}$$
$$\Delta G^o_{25^oC} = -55.9\ \text{kJ/mol}CO_2 \quad (3)$$

The leaching reaction between $C_{12}A_7$ in the slag with Na_2CO_3 generates NaOH. Therefore, they control the $Na_2O_{(caustic)}$ concentration during the leaching so that the $Na_2O_{(caustic)}$ of the solution is within the prescribed "limit" and, subsequently, use the produced $CO^{2-}_{3(aq)}$ to react with the remaining $C_{12}A_7$ phase. Fursman et al. used a leaching solution that consists of 26 g/L of $Na_2O_{(carbonate)}$. On the contrary, we did not introduce CO_2 gas into the solution during the leaching as we used Na_2CO_3 concentration three times higher than they did. As seen in the Reaction (3), the use of CO_2 gas generates $CO^{2-}_{3(aq)}$ in the solution, which means more of free-Na_2CO_3 is available in the system and may accelerate the production of $CaCO_3$-layer at the surface of slag. The $CaCO_3$ layer at the slag's surface is not beneficial to the aluminum extraction extent that is later will be discussed in Section 4.3.

The effect of sodium hydroxide concentration on the alumina dissolution can be explained from a thermodynamic perspective. The Gibbs energy change of Reaction (2) can be written as in Eq. (4).

$$\Delta G_2 = \Delta G_2^\circ + RT \times \ln K_{eq} \quad (4)$$

where $\triangle G_2$ and $\triangle G^\circ{}_2$ are the change of Gibbs energy in Reaction (2) at non–standard and standard condition, respectively. R, T, and K_{eq} are the gas constant, temperature, and equilibrium constant, respectively. The equilibrium constant can be defined by the molar activities (a) ratio between product and reactant of the coexisting phases, which is shown in Eq. (5).

$$K_{eq} = \frac{(a_{NaAlO_2})^{14} \times (a_{NaOH})^{10}}{(a_{Na_2CO_3})^{12} \times (a_{H_2O})^5} \quad (5)$$

If K_{eq} were higher than one, then the $\triangle G_2$ tends to positive values and reaction would move favorably to the left. Likewise, if K_{eq} were lower than one, then the $\triangle G_2$ tends to negative values and reaction would move to the right. The molar activity of an aqueous species is a function of the molar activity coefficient and concentration of the species in the system. Moreover, according to the Le Chatelier principle, if any system at equilibrium is disturbed by changing a parameter affecting it (e.g., concentration) the position of equilibrium moves to counteract the change. In other words, the position of equilibrium would be changed by manipulating the concentration of, for instance, the $Na_2O_{(caustic)}$. The addition of $Na_2O_{(caustic)}$ concentration in the system would shift the equilibrium to the left side of reaction as the K_{eq} value increases, and then decrease the dissolution of alumina to some extent. Another result and discussion on the high $Na_2O_{(caustic)}$ concentration effects on the aluminum extraction based on the phases obtained on the grey mud will be discussed in the Section 4.3.2.

4.3. Characteristics of the grey mud

Results of the BSE cross-section, phase identification, and morphology of the grey mud are presented and discussed in the current section.

4.3.1. Cross-section analysis of the grey mud

The BSE cross-sectional image of the grey mud obtained after the leaching treatment of the slag with 100% $Na_2O_{(carbonate)}$ solution at 45 °C is shown in Fig. 10(a). Next to the figure, an X-ray mapping of several elements of the slag is shown. Subsequently, a normalized WDS point analysis is presented in Table 4. As seen, the grey mud consists of an unreacted slag and a layer that is relatively uniform covering the unreacted slag's surface. Similar to the unleached slag in Fig. 6, the unreacted slag also consists of the primary and secondary phases. The primary phase is indicated as the $C_{12}A_7$ phase, and consists of 46.9 wt% CaO and 52.0 wt% Al_2O_3, on average, with a small number of impurities, i.e., SiO_2, MgO, TiO_2. Meanwhile, the secondary phase consists of 44.1 wt% CaO, 41.0 wt% Al_2O_3, 9.4 wt% SiO_2, 4.9 wt% TiO_2, on average. Moreover, the calcium-containing layer has 50.4 wt% CaO on average, and relatively low Al_2O_3, SiO_2, TiO_2, which is 0.5, 0.2, and 0.4 wt% on average, respectively.

Furthermore, the X-ray mapping element in Fig. 10(b) shows that the formed layer has a higher concentration of Ca and C than that of the unreacted slag. This indicates the layer is a calcium carbonate-containing phase. Also, a small fraction of silicon, titanium, and magnesium elements are detected on the layer as supported by the WDS result in Table 4. It is important to note here that the area of the secondary phase, which is noticeable on the figure from its high concentration of silicon, titanium, and magnesium, also co-exists with the calcium carbonate on the formed layer. This suggests that the secondary phase is a non-leachable phase that remains in its solid phase after the leaching, in which eventually in equilibrium with the calcium carbonate produced from the leaching reaction.

According to the observations above, we propose a leaching mechanism of a calcium aluminate slag that has both leachable and non-leachable phases, which is shown schematically in Fig. 11.

The leaching mechanism can be divided to three main stages:

(a) The initial stage. The slag consists of a leachable $C_{12}A_7$ phase (shown as number 1) and non-leachable Ca-Al-Si-Ti bearing phase (shown as number 2). At this stage, the leaching reactions occur at the surface of slag particles between the leachable phase and the sodium carbonate solution. In a solid/liquid reaction, a boundary layer is created between the interfaces of the surface with the bulk fluid. The boundary layer is the layer of medium that is not very mobile due to solvent molecules are bound to the surface, and layers of solvent molecules near the surface tend to associate with surface and near-surface molecules (Free, 2013). That is to say, it is essential for the leaching reactions to start by transporting the ionic species (CO_3^{2-}, Na^+) through the bulk fluid towards to adjacent of the surface of the slag and subsequently followed by diffusing the ions through the boundary layer. Furthermore, the products of the leaching reaction are $CaCO_3$ (shown as number 3), $NaAlO_2$, and NaOH. As shown in the WDS result in Table 4, it is confirmed that the $C_{12}A_7$ phase contains small impurities, e.g., SiO_2. We suggest that the impurities are small (submicron) intrusions of the secondary phase in the primary one that is difficult to observe by SEM. Also, we propose that as the leachable phases digested, the impurities are “liberated” from the phase, and therefore, dissolved in the pregnant liquid solution as aqueous phases.

(b) The $CaCO_3$ growth stage. According to the leaching Reactions (1) and (2), the $CaCO_3$ is the only solid product produced from the

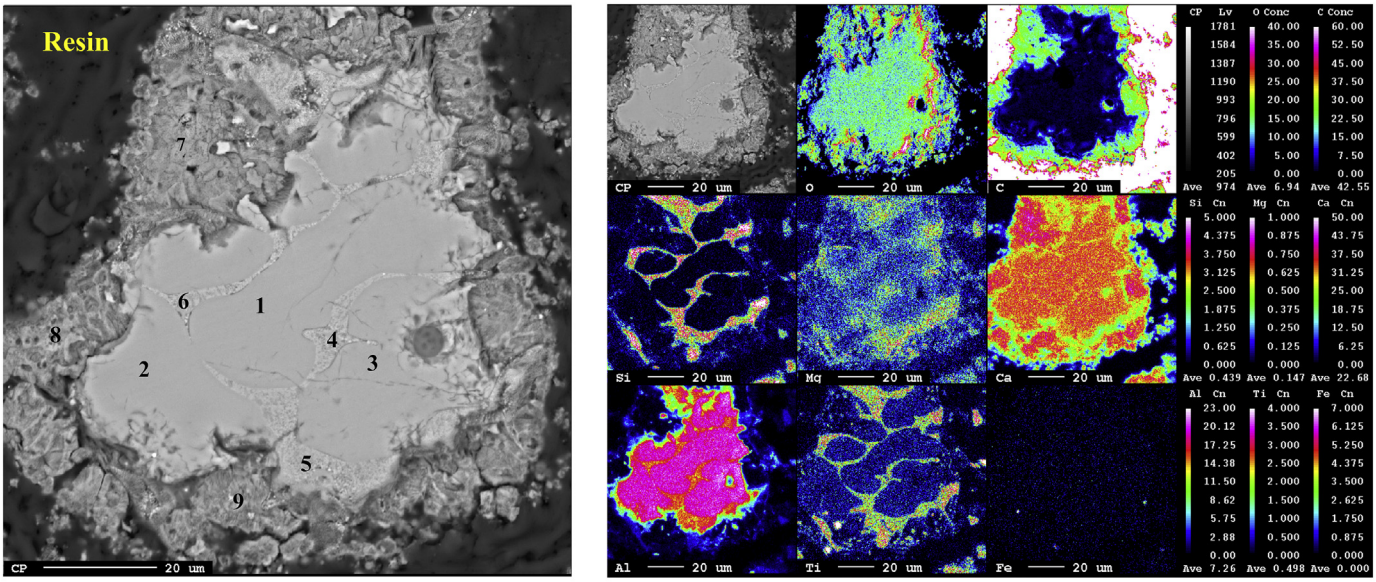

Fig. 10. Image of the cross-section of grey mud obtained: (a) BSE of grey mud, and (b) X-ray mapping of several elements after the leaching treatment of the slag in 100%$Na_2O_{(carbonate)}$ solution, at 45 °C and 1 atm in 30 min.

Table 4
A normalized WDS point analysis.

Points	CaO (wt%)	Al_2O_3 (wt%)	SiO_2 (wt%)	MgO (wt%)	P_2O_5 (wt%)	TiO_2 (wt%)	MnO (wt%)	FeO (wt%)	CO_2[a](wt%)
1–3	46.9	52.0	0.2	0.2	2×10^{-2}	0.6	NA	2×10^{-2}	NA
4–6	44.1	41.0	9.4	0.5	1×10^{-2}	4.9	4×10^{-2}	3×10^{-2}	NA
7–9	50.4	0.5	NA	NA	NA	NA	NA	NA	48.3

[a] Where CO_2 in carbonate phase.

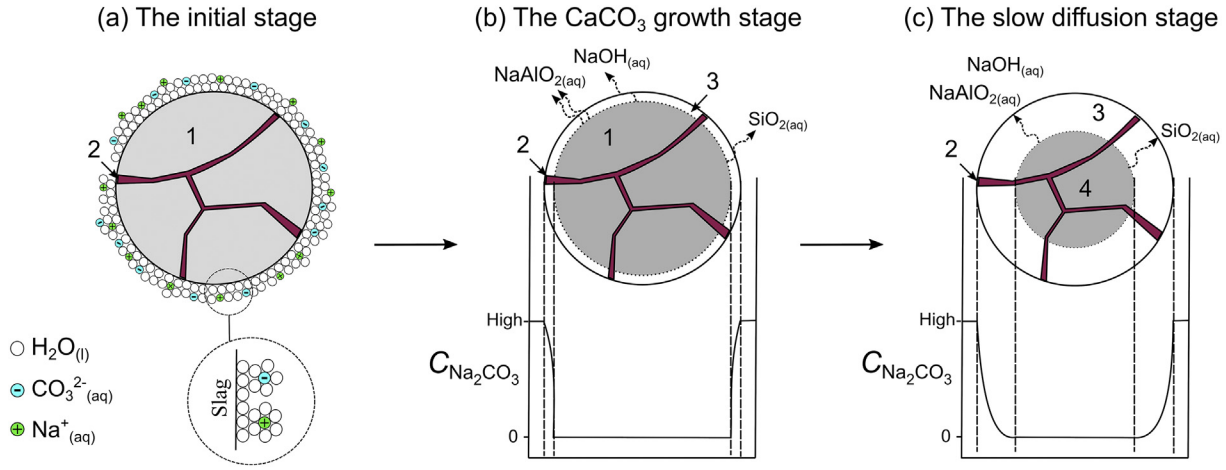

Fig. 11. The leaching mechanism of a slag that consists of three stages; the initial, the $CaCO_3$ growth, and the slow diffusion stages. Legend: 1. Leachable mayenite phase; 2. Unleachable Ca-Al-Si-Ti bearing phase; 3. $CaCO_3$; 4. Unreacted slag.

leaching. It nucleates and grows on a substrate, which is the surface of the slag. The $CaCO_3$ grows uniformly and forms a passive layer. Due to the formation of this passive layer, the Na_2CO_3 concentration may decrease gradually from the outer surface of the layer until the surface of the unreacted slag. On the other hand, the unleached phase remains in its solid phase, as the phase does not react with the Na_2CO_3.

(c) The slow diffusion stage. The Na_2CO_3 diffuses slowly through the layer, as the medium is relatively dense. However, we can see in Fig. 9 that the layer has some visible cracks that may allow the Na_2CO_3 propagate to the core. If there is no new crack-path nor pores formed during the leaching, thus, in the end, we may assume that there is a stage when Na_2CO_3 does not suffice for the leaching reaction on the surface of the unreacted slag (shown as number 4). When this stage happens then, the leaching extent progresses slowly, and the amount of mass transfer from the unreacted slag to the pregnant liquid solution is negligible.

4.3.2. Phases of the grey mud

The XRD results of the grey mud in Fig. 12 confirms the calcium-containing layer is the $CaCO_3$ phase that is either in the form of calcite or vaterite. We do not observe the peaks of vaterite on the grey mud obtained from $Na_2O_{(caustic)}$-addition solution. We suggest that the formation of vaterite or calcite are affected by the $Na_2O_{(caustic)}$ concentration of the system, i.e., pH., which is in agreement with the literature (Söhnel and Mullin, 1982). Moreover, the remaining peaks are $C_{12}A_7$ and C_5A_3 as the unleached slag. The formation of $CaCO_3$ on the slag's surface gives valuable information on the leaching behavior of the slag. The passive layer of $CaCO_3$ does not react with the leaching agent Na_2CO_3, which slows the leaching Reactions (1) and (2) to occur as mentioned in the previous section; hence we may say that the reaction is diffusion rate limiting.

Another interesting observation from the XRD result is the precipitation of $Ca_3Al_2(OH)_{12}$ (denoted as $3CaO{\cdot}Al_2O_3{\cdot}6H_2O$) phase in the residue obtained from the leaching solution that contains 25 to 50% $Na_2O_{(caustic)}$. The $3CaO{\cdot}Al_2O_3{\cdot}6H_2O$ phase is a hydrogarnet solid phase that theoretically consists of 26.9 wt% Al_2O_3. The precipitation of the phase causes loss of alumina during the leaching. The high content of $Na_2O_{(caustic)}$ appears to be the main reason why the hydrogarnet phase precipitates, which is in agreement with the result from literature (Lundquist and Leitch, 1963a, 1963b). The literature stated that as the carbonate ion concentration in the solution increased from 0 to 100%, the amount of $3CaO{\cdot}Al_2O_3{\cdot}6H_2O$ precipitated showed a corresponding decrease, and $CaCO_3$ was precipitated instead. In other words, if the leaching system has a high $Na_2O_{(carbonate)}$ concentration of the total alkali, wherein this study is higher than 85%, then the $CaCO_3$ is favorably precipitated instead of $3CaO{\cdot}Al_2O_3{\cdot}6H_2O$ phase. The carbonate anions in the solution react with the calcium cations from the depolymerization of the calcium aluminate slag. Likewise, if the number of carbonate anions is insufficient, then the dissolved aluminum species reacts with the calcium cations and produce $3CaO{\cdot}Al_2O_3{\cdot}6H_2O$.

Moreover, Table 5 shows the XRF analysis of the grey mud produced from 45, 60, and 75 °C leaching temperature in 100% $Na_2O_{(carbonate)}$ solution. The composition is shown after a loss on ignition (LOI) test by heating the grey mud inside a muffle furnace at 950 °C, air atmosphere, for about one hour. The tests resulted in 21.2 wt% of mass losses on average, which is due to the decomposition of $CaCO_3$ to CaO and $CO_{2(g)}$. The primary phase of the grey mud is CaO and then followed by a relatively low amount of Al_2O_3 (7 ± 1 wt%).

4.3.3. Morphology of the grey mud

The morphology of different grey muds has been investigated and is shown in Fig. 13. Fig. 13(a) and (b) show the morphology of grey mud (hereafter named GM-A) produced from 100% $Na_2O_{(carbonate)}$ solution at 45 °C and 1 atm in 1000× and 3000× magnification, respectively. Meanwhile, Fig. 12(c) and (d) are the morphology of other grey mud (hereafter named GM-B) produced from 50:50 concentration ratio of $Na_2O_{(carbonate)}$:$Na_2O_{(caustic)}$ solution in 1000× and 2000× magnification, respectively.

The GM-A consists of calcite and vaterite crystals. A calcite crystal has a cubical shape, whereas vaterite has a spherical one (Ni and Ratner, 2008; Wang et al., 2013). Vaterite is the least stable

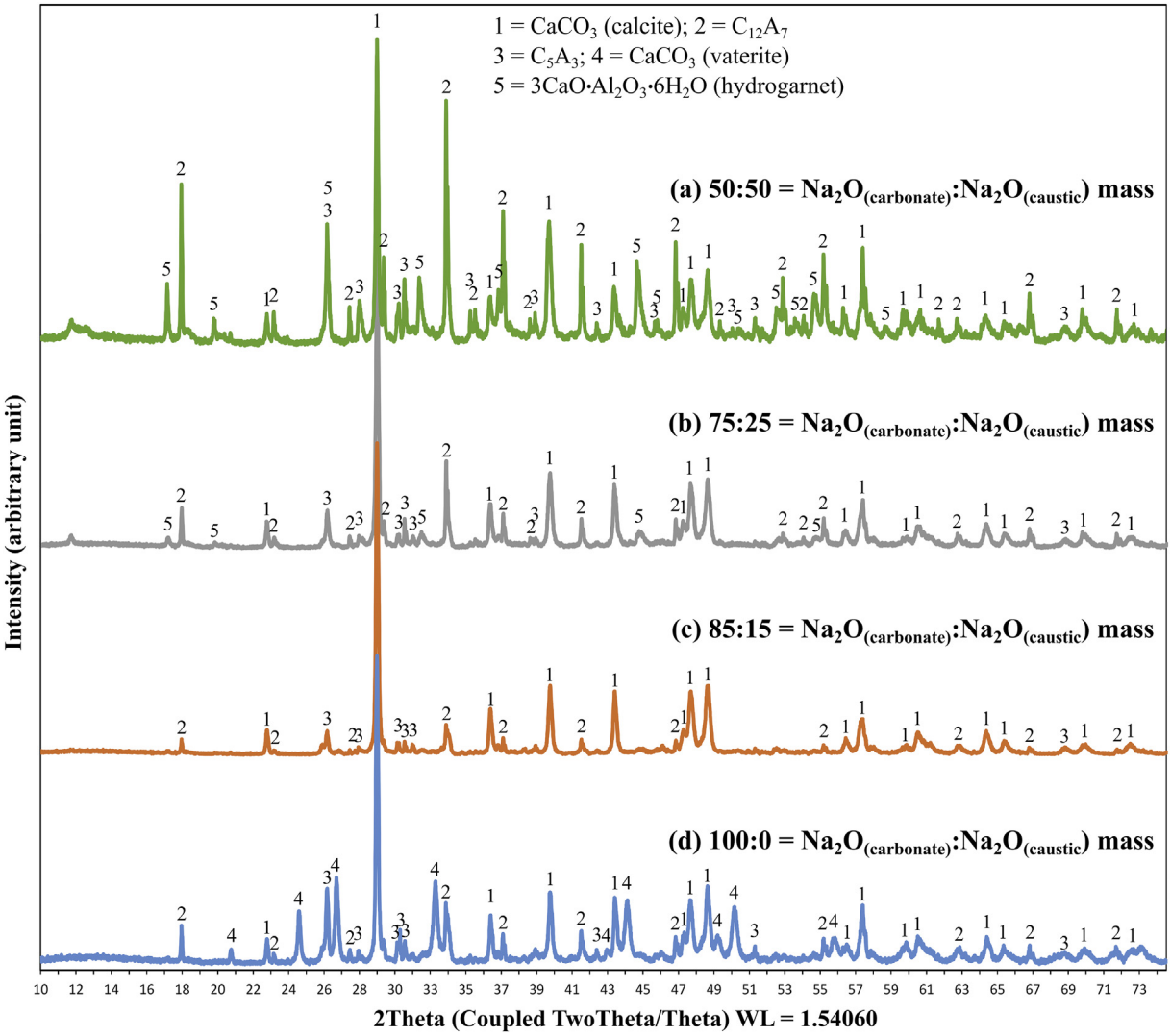

Fig. 12. XRD patterns of the grey muds obtained from the leaching treatment of the slag in 60 g/L Na_2O, at 45 °C, 1 atm, in 30 min under different concentration ratios of $Na_2O_{(carbonate)}$:$Na_2O_{(caustic)}$; (a) 50:50, (b) 75:25, (c) 85:15, (d) 100:0.

Table 5
The XRF analysis of grey mud after an LOI test.

Constituents	Leaching temperature		
	45 °C (wt%)	60 °C (wt%)	75 °C (wt%)
CaO	64.0	57.9	63.8
Al_2O_3	7.8	5.9	5.9
SiO_2	2.2	1.8	1.7
TiO_2	2.9	3.1	3.1
Na_2O	2.2	2.1	2.1
Fe_2O_3	1.0	1.3	1.5
MgO	0.6	0.5	0.5
P_2O_5	0.1	4.2×10^{-2}	1.1×10^{-2}
V_2O_5	4.3×10^{-2}	3.5×10^{-2}	3.3×10^{-2}
Cr_2O_3	5.9×10^{-2}	5.3×10^{-2}	5.9×10^{-2}
MnO	6.4×10^{-2}	6.5×10^{-2}	6.4×10^{-2}
LOI	17.7	25.9	19.9

thermodynamic form of $CaCO_3$ compared to other polymorphs (e.g., aragonite and calcite) (Ni and Ratner, 2008). However, the polymorphs could exist at the same time depending on the condition and kinetics of the transformation (Dickinson and McGrath, 2004). In an aqueous solution, vaterite can transform to aragonite in 60 min at 60 °C and to calcite in 24 h at room temperature as demonstrated by Ogino et al. (1987).

On the other hand, the GM-B consists of calcite, and a fibrous-like shape, which incorporates and forming a network structure to other grains. The fibrous-like shape does not resemble the morphology of any un-hydrated $CaCO_3$ polymorphs, i.e., vaterite, aragonite, and calcite. Also, the fibrous-like shape does not resemble a morphology of typical hydrogarnet crystal, which is an octahedral according to the literature (Kyritsis et al., 2009). However, an observation of the interaction between kaolinite ($Al_2Si_2O_5(OH)_4$) and portlandite ($Ca(OH)_2$) solution made by Donchev et al. (Donchev et al., 2010) showed that fine-needle and fibrous-like products could be interconnected with hydrogarnet crystals. They have assumed that the fibrous-like product is a mixture of primarily formed gehlenite hydrate ($2CaO{\cdot}Al_2O_3{\cdot}SiO_2{\cdot}8H_2O$), hydrogarnet, and calcium-silicate-hydrate gel. Thus, it is very likely that the fibrous-like shape of the GM-B in the current study is a calcium-silicate-hydrate phase that incorporates the hydrogarnet crystals.

5. Conclusion

The leaching treatment of a ternary CaO-Al_2O_3-SiO_2 slag produced from smelting-reduction of low-grade bauxite was carried out at 45, 60, and 75 °C and 1 atm in 30 min with different proportion $Na_2O_{(carbonate)}$ and $Na_2O_{(caustic)}$ with a fixed liquid-solid ratio 20 mL/g and

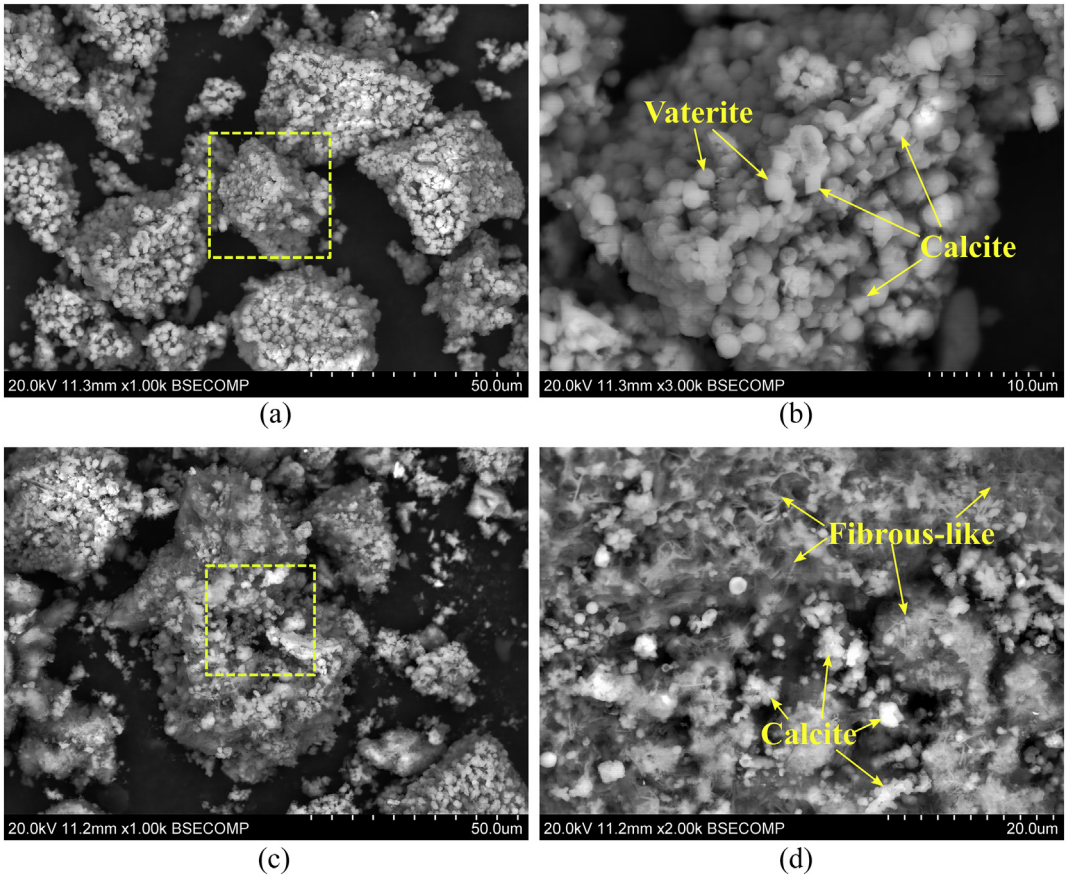

Fig. 13. BSE images of the morphology of the grey mud obtained after leaching of the slag in the 100% $Na_2O_{(carbonate)}$ solution at 45 °C in 30 min, in (a) 1000× and (b) 3000× magnification. Meanwhile, (c) and (d) are BSE images of grey mud obtained after leaching of the slag in the 50:50 $Na_2O_{(carbonate)}$:$Na_2O_{(caustic)}$ solution in 1000 and 2000× magnification, respectively.

concentration of 60 g/L Na_2O. The leaching characteristics can be summarized as follows:

(1) The leaching reaction of calcium-aluminate phases in a sodium carbonate solution is fast and temperature gives mild effect to the aluminum extraction in the first 30 min of the reaction.
(2) The addition of $Na_2O_{(caustic)}$ in the solution decreases the aluminum dissolution of the slag, while it increases the silicon dissolution into the pregnant liquid solution.
(3) The calcite-containing layer formed and distributed around the surface of the slag as the leaching reactions progress.
(4) The kinetics of leaching reaction appears to be diffusion rate limited as the passive calcium carbonate-containing layer formed at the unreacted surface of slag and may inhibit the progress of leaching reactions.

The results obtained from the current study may pave a new way to utilize CaO-Al_2O_3-SiO_2 slag more effectively. The slow diffusion of Na_2CO_3 to the unreacted $12CaO{\cdot}7Al_2O_3$ phase due to the formation of the calcite-containing layer at the surface of slag is suggested to be the reaction limiting. Therefore, leaching that employs a mechanochemical treatment such as wet grinding, or a sonochemical treatment using ultrasound, can be used to break the layer during the leaching. Such treatments may allow the Na_2CO_3 diffuse to and attack the unreacted $12CaO{\cdot}7Al_2O_3$, and achieve a high aluminum extraction extent.

Acknowledgement

The NTNU has funded the research and supported by the Research Domain 5 – Materials and the Society in SFI Metal Production (Project no. 237738). The School of Mining and Metallurgical Engineering, NTUA, is acknowledged for the use of leaching reactor, ICP-OES, and XRF analyzer. The scientific support from the ENSUREAL Horizon 2020 project is also acknowledged.

Appendix A. Supplementary data

Supplementary data to this article can be found online at https://doi.org/10.1016/j.hydromet.2019.105184.

References

Azof, F.I., Kolbeinsen, L., Safarian, J., 2017. The Leachability of Calcium Aluminate Phases in Slags for the Extraction of Alumina, in: Travaux 46, Proceedings of 35th International ICSOBA Conference. ICSOBA, Hamburg, pp. 243–253.
Azof, F.I., Kolbeinsen, L., Safarian, J., 2018. Characteristics of calcium-aluminate slags and pig Iron produced from smelting-reduction of low-grade bauxites. Metall. Mater. Trans. B Process Metall. Mater. Process. Sci. 49, 2400–2420. https://doi.org/10.1007/s11663-018-1353-1.
Azof, F.I., Kolbeinsen, L., Safarian, J., 2019a. Kinetics of the leaching of alumina-containing slag for alumina recovery. Proc. EMC 2019, 511–526.
Azof, F.I., Yang, Y., Panias, D., Kolbeinsen, L., Safarian, J., 2019b. Leaching characteristics and mechanism of the synthetic calcium-aluminate slags for alumina recovery. Hydrometallurgy 185, 273–290. https://doi.org/10.1016/j.hydromet.2019.03.006.
Blake, H.E., Fursman, O.C., Fugate, A.D., Banning, L.H., 1966. Adaptation of the Pedersen Process to the Ferruginous Bauxites of the Pacific Northwest. Bureau of Mines US Department of the Interior.
Calagari, A.A., Abedini, A., 2007. Geochemical investigations on Permo-Triassic bauxite horizon at Kanisheeteh, east of Bukan, West-Azarbaidjan, Iran. J. Geochem. Explor. 94, 1–18. https://doi.org/10.1016/j.gexplo.2007.04.003.
Company, Norsk Aluminium, 1944a. Process for the Production of Calcium Aluminate Slags Containing Less Than Approximately 10 Percent Silica. pp. 67696.
Company, Norsk Aluminum, 1944b. Process for the Production of Calcium Aluminate Slags Containing more Than 10 Percent Silica. pp. 67695.
Dickinson, S.R., McGrath, K.M., 2004. Aqueous precipitation of calcium carbonate

modified by hydroxyl-containing compounds. Cryst. Growth Des. 4, 1411–1418. https://doi.org/10.1021/cg049843i.
Donchev, I., Ninov, J., Doykov, I., Petrova, N., Dimova, L., 2010. On the formation of cement phases in the course of interaction of kaolinite with portlandite. J. Univ. Chem. Technol. Metall. 45, 391–396.
Free, M.L., 2013. Hydrometallurgy: Fundamentals and Applications. John Wiley & Sons, Inc, New Jersey.
Fursman, O.C., Blake Jr., H.E., Mauser, J.E., 1968. Recovery of Alumina and Iron from Pacific Northwest Bauxites by the Pedersen Process. (Albany).
Hudson, L.K., Misra, C., Perrotta, A.J., Wefers, K., Williams, F.S., 2000. Aluminum Oxide, in: Ullmann's Encyclopedia of Industrial Chemistry. Wiley-VCH Verlag GmbH & Co, KGaA, Weinheim, Germany. https://doi.org/10.1002/14356007.a01_557.
Kusrini, E., Harjanto, S., Herdino, F., Prasetyanto, E., Rahman, A., 2018. Effect of mechanochemical and roasting techniques for extraction of rare earth elements from Indonesian low-grade bauxite. IOP Conf. Ser. Mater. Sci. Eng. 316, 012025. https://doi.org/10.1088/1757-899X/316/1/012025.
Kyritsis, K., Meller, N., Hall, C., 2009. Chemistry and morphology of hydrogarnets formed in cement-based CASH hydroceramics cured at 200° to 350°C. J. Am. Ceram. Soc. 92, 1105–1111. https://doi.org/10.1111/j.1551-2916.2009.02958.x.
Laskou, M., Economou-Eliopoulos, M., Mitsis, I., 2005. Bauxite ore as an energy source for bacteria driving iron-leaching and bio-mineralization. Hell. J. Geosci. 45, 163–174.
Liu, W., Yang, J., Xiao, B., 2009. Review on treatment and utilization of bauxite residues in China. Int. J. Miner. Process. 93, 220–231. https://doi.org/10.1016/j.minpro.2009.08.005.
Lundquist, R.V., Leitch, H., 1963a. Solubility characteristics of monocalcium aluminate. US Dept. Inter. Bur. Mines 6294, 1–9.
Lundquist, R.V., Leitch, H., 1963b. Two hydrated calcium aluminates encountered in the lime-soda sinter process. US Dept. Inter. Bur. Mines 6335.
Ni, M., Ratner, B.D., 2008. Differentiating calcium carbonate polymorphs by surface analysis techniques-an XPS and TOF-SIMS study. Surf. Interface Anal. 40, 1356–1361. https://doi.org/10.1002/sia.2904.
Nielsen, K., 1978. The pedersen process - an old process in a new light. Erzmetall 31, 523–525.
Norway"s Norsk Hydro apologises for spills in Brazil river_2018.pdf WWW Document, 2018. The Local. URL. https://thelocal.no/20180319/norways-norsk-hydro-apologises-for-spills-in-brazil-river (accessed 8.14.18).
Ogino, T., Suzuki, T., Sawada, K., 1987. The formation and transformation mechanism of calcium carbonate in water. Geochim. Cosmochim. Acta 51, 2757–2767. https://doi.org/10.1016/0016-7037(87)90155-4.
Outrage as plant bosses acquitted over fatal toxic spill in Hungary WWW Document, 2016. Guard. URL. https://www.theguardian.com/world/2016/jan/28/outrage-plant-bosses-acquitted-fatal-toxic-spill-hungary (accessed 8.14.18).
Pedersen, H., 1927. Process of Manufacturing Aluminum Hydroxide. pp. 1618105.
Safarian, J., 2018a. Hydrometallurgical processes at NTNU for sustainable production of feedstock for aluminum and solar industries. In: 4th Hydrometallurgy Seminar, (Oslo).
Safarian, J., 2018b. Extraction of iron and ferrosilicon alloys from low-grade bauxite ores. In: Davis, B. (Ed.), Extraction. 2018. pp. 825–837. https://doi.org/10.1007/978-3-319-95022-8_66.
Safarian, J., Kolbeinsen, L., 2016a. Sustainability in alumina production from bauxite. In: Sustainable Industrial Processing Summit, pp. 75–82.
Safarian, J., Kolbeinsen, L., 2016b. Smelting-reduction of bauxite for sustainable alumina production. In: Sustainable Industrial Processing Summit, pp. 149–158.
Sellaeg, H., Kolbeinsen, L., Safarian, J., 2017. Iron separation from bauxite through smelting-reduction process. In: Minerals, Metals and Materials Series, pp. 127–135. https://doi.org/10.1007/978-3-319-51541-0_19.
Smith, P., 2009. The processing of high silica bauxites - review of existing and potential processes. Hydrometallurgy. https://doi.org/10.1016/j.hydromet.2009.04.015.
Söhnel, O., Mullin, J.W., 1982. Precipitation of calcium carbonate. J. Cryst. Growth 60, 239–250. https://doi.org/10.1016/0022-0248(82)90095-1.
Tsesmelis, K., 2017. Bauxite mine rehabilitation & bauxite residue management: a global perspective. In: Proceedings of 35th International ICSOBA Conference. ICSOBA, pp. 71.
Vafeias, M., Marinos, D., Panias, D., Safarian, J., van Der Eijk, C., Solhem, I., Balomenos, E., Ksiazek, M., Davris, P., 2018. From red to grey: revisiting the Pedersen process to achieve holistic bauxite ore utilisation. In: Proceedings of the 2nd International Bauxite Residue Valorisation and Best Practices Conference, pp. 111–117.
Wang, H., Alfredsson, V., Tropsch, J., Ettl, R., Nylander, T., 2013. Formation of CaCO3 deposits on hard surfaces—effect of bulk solution conditions and surface properties. ACS Appl. Mater. Interfaces 5, 4035–4045. https://doi.org/10.1021/am401348v.
Zarasvandi, A., Zamanian, H., Hejazi, E., 2010. Immobile elements and mass changes geochemistry at Sar-Faryab bauxite deposit, Zagros Mountains, Iran. J. Geochem. Explor. 107, 77–85. https://doi.org/10.1016/j.gexplo.2010.06.007.